

1 ***In silico* screening of TMPRSS2 SNPs that affect its binding with SARS-**  
2 **CoV2 spike protein and directly involved in the interaction affinity changes**

3 Fatma Nouira<sup>1</sup>, Manel Hamdi<sup>1</sup>, Alaeddine Redissi<sup>1</sup>, Soumaya Kouidhi<sup>1</sup>, Cherine  
4 Charfeddine<sup>1</sup>, Meriem M'saad<sup>2</sup>, Ameer Cherif<sup>1</sup>, Sabri Messaoudi<sup>3,4</sup>, Sarah Aldulaijan<sup>1\*5</sup>,  
5 Nouredine Raouafi<sup>6</sup>, Adnene Dhouib<sup>3</sup> and Amor Mosbah<sup>1\*</sup>

6 <sup>1</sup> Laboratory (BVBGR)-LR11ES31, Univ. Manouba, ISBST, Biotechnopole Sidi Thabet,  
7 2020, Ariana, Tunisia. [nourifatma.sv3@gmail.com](mailto:nourifatma.sv3@gmail.com) (N.F), [hamdimanel511@gmail.com](mailto:hamdimanel511@gmail.com)  
8 (M.H), [redissialadin@gmail.com](mailto:redissialadin@gmail.com) (A.R), [soumaya.kouidhi@isbst.uma.tn](mailto:soumaya.kouidhi@isbst.uma.tn) (S.K),  
9 [cherine.charfeddine@gmail.com](mailto:cherine.charfeddine@gmail.com) (C.C), [ameur.cherif@uma.tn](mailto:ameur.cherif@uma.tn) (A.C) and  
10 [amor.mosbah@isbst.uma.tn](mailto:amor.mosbah@isbst.uma.tn) (A.M)

11 <sup>2</sup> Laboratory of Biotechnology and Nuclear Technologies LR16CNSTN01, National Centre  
12 for Nuclear Sciences and Technology, Technopole de Sidi Thabet, Sidi Thabet T-2020,  
13 Tunisia. [msaad\\_tn@yahoo.fr](mailto:msaad_tn@yahoo.fr) (M.M)

14 <sup>3</sup> Faculty of Sciences of Bizerte FSB, University of Carthage, 7021 Jarzouna, Tunisia.

15 <sup>4</sup> Department of Chemistry, College of Science, Qassim University, Buraidah 51452, Saudi  
16 Arabia. [sabri\\_messaoudi@yahoo.fr](mailto:sabri_messaoudi@yahoo.fr) (S.M)

17 <sup>5</sup> Department of Chemistry, College of Science, Imam Abdulrahman Bin Faisal  
18 University, Dammam, 31113, Saudi Arabia. [saaldulaijan@gmail.com](mailto:saaldulaijan@gmail.com) (S.A) and  
19 [addhouib@gmail.com](mailto:addhouib@gmail.com) (A.D)

20 <sup>6</sup> Sensors and Biosensors Group, Laboratory of Analytical Chemistry & Electrochemistry  
21 (LR99ES15), Faculty of Science, University of Tunis El Manar, 2092 Tunis El Manar,  
22 Tunis, Tunisia. Email : [nouredine.raouafi@fst.utm.tn](mailto:nouredine.raouafi@fst.utm.tn) (N.R)

23 \*: Corresponding authors e-mails: [amor.mosbah@isbst.uma.tn](mailto:amor.mosbah@isbst.uma.tn) (A.M);  
24 [saaldulaijan@gmail.com](mailto:saaldulaijan@gmail.com) (S. A)

26

## 27 **Abstract**

28 In this paper, we used in silico analysis to shed light on the possible interaction between  
29 TMPRSS2 and SARS-CoV2 spike (S) protein by examining the role of TMPRSS2 single  
30 nucleotide polymorphisms (SNPs) in relation with susceptibility and inter-individual  
31 variability of SARS-CoV2 infection. First, we used molecular docking of human  
32 TMPRSS2 protein to predict the binding site of TMPRSS2, especially the TMPRSS2 link  
33 loops, in order to assess the effect TMPRSS2 SNPs. The latter lead to missense variants  
34 on the interaction between TMPRSS2 and SARS-CoV2 S protein. In a second step, we  
35 further refine our analysis by performing a structure-function analysis of the complexes  
36 using PyMol software, and finally by MD simulations to validate the as-obtained results.  
37 Our findings show that 17 SNPs among the 692 natural TMPRSS2 coding variants are in  
38 positions to influence the binding of TMPRSS2 with the viral S protein. All of them give  
39 more important interaction energy as assessed by docking. Among the 17 SNPs, four  
40 missense variants E389A, K392Q, T393S and Q438E lead to “directly increasing” the  
41 interaction affinity and 2 missense variants R470I and Y416C cause it “directly  
42 decreasing”. The R470I and Y416C present in African and American population,  
43 respectively. While the other 4 SNP variants (E389A; K392Q; T393S and Q438E) are  
44 present only in the European population, which could link the viral infection  
45 susceptibility to demographic, geographic and genetic factors.

## 46 **KEYWORDS**

47 COVID-19; Single nucleotide polymorphisms; TMPRSS2; Spike protein; Docking;  
48 Molecular Dynamics

49

## 50 INTRODUCTION

51 The pathogenesis of the coronavirus disease (COVID-19) is triggered by the entry of  
52 SARS-CoV<sub>2</sub> via the spike protein into angiotensin-converting enzyme 2 (ACE<sub>2</sub>)-bearing  
53 host cells, especially pneumocytes, resulting in overactivation of the immune system  
54 (cytokine storm), which attacks the infected cells and damages the lung tissue ([Hakmi  
55 et al.,2020](#)). Cell entry of the betacoronaviruses, depends on the binding of the surface  
56 unit, S<sub>1</sub>, of the viral spike protein to ACE<sub>2</sub> receptor, which facilitates viral attachment to  
57 the surface of the target cells. Moreover, to fuse membranes, the S protein needs to be  
58 proteolytically activated at the S<sub>1</sub>/S<sub>2</sub> boundary, such that S<sub>1</sub> dissociates and S<sub>2</sub> undergoes  
59 a radical structural modification, therefore, viral entry requires not only the binding to  
60 the ACE<sub>2</sub> receptor but also the priming of the viral S protein by the transmembrane  
61 protease serine 2 (TMPRSS<sub>2</sub>), which cleaves the S proteins at the S<sub>1</sub>/S<sub>2</sub> and S<sub>2</sub> sites  
62 ([Hoffman et al., 2020](#); [Baughn et al., 2020](#)). This step is mandatory for the virus-host cell  
63 membrane fusion and cell entry ([Hoffman et al., 2020](#); [Matsuyama et al., 2020](#)).

64 TMPRSS<sub>2</sub> is an essential enzyme that can cleave hemagglutinin of many subtypes of the  
65 influenza virus and the coronavirus S protein including severe acute respiratory  
66 syndrome-related coronavirus (SARS-CoV) ([Hoffmann et al., 2020](#)) and the Middle East  
67 respiratory syndrome-related coronavirus (MERS-CoV) ([Du et al., 2017](#)), thus facilitating  
68 the virus-cell membrane fusion and viral infection ([Böttcher et al., 2006](#)). *Matsuyama et*  
69 *al.* demonstrated that TMPRSS<sub>2</sub>-expressing cell lines are highly susceptible to SARS-  
70 CoV, MERS-CoV, and SARS-CoV<sub>2</sub> ([Matsuyama et al., 2020](#)), which proves that *TMPRSS<sub>2</sub>*  
71 expression is crucial for the spread of the virus and pathogenesis. Results from several  
72 studies on prostate cancer revealed that overexpression of *TMPRSS<sub>2</sub>* induced by  
73 transactivation of androgen receptor caused growth, invasion and metastasis of prostate  
74 cancer stem cells ([Chen et al., 2019](#); [Ko et al., 2015](#)). Recently, a plethora of evidence  
75 showed that single nucleotide polymorphisms (SNPs) in *TMPRSS<sub>2</sub>* gene may be involved  
76 in several disorders including prostate and breast cancers via modulation of *TMPRSS<sub>2</sub>*  
77 expression ([Bhanushali et al., 2018](#); [Luostari et al., 2014](#)). As a result, genetic variation in  
78 this gene may modulate genetic predisposition to infection and virus clearance in the  
79 host.

80 Most recently, the ongoing COVID-19 pandemic has created the hypothesis that inter-  
81 individual genetic differences may affect the spatial transmission dynamics of SARS-  
82 CoV2, the susceptibility and severity of disease, and the inflammatory and immune  
83 response ([Paniri et al., 2020](#)). Specifically, there is evidence that the TMPRSS2 plays a  
84 crucial role in SARS-CoV2 infection and it was speculated that *TMPRSS2* gene  
85 polymorphism may modulate the interaction between TMPRSS2 and the virus spike  
86 protein during the virus entry into the host cell and may influence individual's  
87 susceptibility to the virus infection ([Paniri et al., 2020](#); [David et al., 2020](#); [Singh et al.,](#)  
88 [2020](#)). Furthermore, recent studies used statistical analysis and *in silico* tools to predict  
89 possible impact of an amino acid substitution/deletion on the structure and function of  
90 a given human protein to identify variants that could result in TMPRSS2 loss of  
91 structure/function and suggested that these variants may indirectly modulate the  
92 interaction affinity between TMPRSS2 and the invading virus ([Zarubin et al., 2020](#);  
93 [Vashnubhotla et al., 2020](#)).

94 In this study, we used several bioinformatics tools and databases for a computational  
95 analysis of TMPRSS2 to determine the role of single nucleotide polymorphisms in  
96 susceptibility and inter-individual variability of SARS CoV2 infection by examining the  
97 effect of TMPRSS2 SNPs on the interaction of this protein with the S<sub>1</sub>/S<sub>2</sub> domain of the  
98 spike protein. However, the molecular structure of human TMPRSS2 protein is not  
99 available in the protein database (PDB) and structural details of intermolecular  
100 interactions between SARS-CoV2 and TMPRSS2 are not very clear. So, we built the  
101 TMPRSS2 3D structure using I-TASSER, we predicted the binding site of TMPRSS2  
102 protein, more specifically, all TMPRSS2 link loops and we have used *in silico* molecular  
103 docking to analyze the possible effects of TMPRSS2 SNPs leading to missense variants  
104 on the interaction between TMPRSS2 and the viral S protein. To further refine our  
105 analysis, we performed a structure function analysis of the complexes obtained by  
106 molecular docking using PyMol software ([DeLano et al., 2002](#)), followed by MD  
107 simulations using NAMD2 and VMD visualization software ([Humphrey et al., 1996](#);  
108 [Phillips et al., 2005](#)) to validate the results obtained. To sum up, the idea of this approach  
109 is to detect the TMPRSS2 polymorphisms affecting binding interfaces, and which are  
110 directly associated with the increase or decrease of the interaction affinity with the S<sub>1</sub>/S<sub>2</sub>

111 domain of the spike protein, which can be considered as protective or susceptibility  
112 variants to SARS CoV-2 infection.

## 113 **MATERIAL AND METHODS**

### 114 **TMPRSS2 polymorphism analysis**

115 SNPs in *TMPRSS2*, with minor allele frequency (MAF) between 0.01 and 0.5, were  
116 extracted from Ensembl genome browser (<https://asia.ensembl.org/index.html>)  
117 (Cunningham et al., 2019), gnomAD (<https://gnomad.broadinstitute.org/>) (Karczewski  
118 et al, 2020) , 1000 Genomes ([https://www.internationalgenome.org/1000-genomes-](https://www.internationalgenome.org/1000-genomes-browsers/)  
119 [browsers/](https://www.internationalgenome.org/1000-genomes-browsers/)) (Siva, 2008), and NHLBI (<https://evs.gs.washington.edu/EVS/>) (Auer et al.,  
120 2012) databases. Appropriate filters were employed to limit the data to only the missense  
121 and damaging SNPs of *TMPRSS2*. The functional impact of allelic variants of *TMPRSS2*  
122 was predicted using sorting intolerant from tolerant (SIFT) ([https://sift.bii.a-](https://sift.bii.a-star.edu.sg/)  
123 [star.edu.sg/](https://sift.bii.a-star.edu.sg/)), which predicts the effects of amino acids substitution on protein structure,  
124 the score ranges of 0 to 0.05 are considered as deleterious substitutions (Ng et al., 2003),  
125 PolyPhen-2(<http://genetics.bwh.harvard.edu/pph2/>), is a useful database that predicts  
126 the possible consequences of amino acid substitution on functional and structural  
127 proteins. Score range of 0.0 – 0.15, 0.15 – 0.85 and 0.85 – 1.0 are considered benign,  
128 possibly damaging and damaging, respectively (Adzhubei et al., 2013). Combined  
129 annotation-dependent depletion (CADD) (<https://cadd.gs.washington.edu>) is a tool  
130 used to assess the harmfulness of single nucleotide variants in the human genome.  
131 Variants with CADD scores > 20 are considered deleterious variants (Rentzsch et al.,  
132 2019).

### 133 **Protein molecular modelling**

134 When this study was started, the crystal structure of human *TMPRSS2* has not been filed  
135 in the Protein Data Bank (PDB), therefore, we modelled the structure of human  
136 *TMPRSS2* employing I-TASSER (Iterative Threading Assembly Refinement), which is a  
137 strong predictor of protein 3D structure, aiming to determine by computational  
138 calculations the spatial location of every atom in a protein molecule from the amino acid  
139 sequence (Zhang, 2008). In April 2021, the crystal structure of human *TMPRSS2* in  
140 complex with Nefamostat has been deposited in the Protein Data Bank (code PDB:

141 7MEQ), we compared our structure to the one recently deposited in PDB in order to  
142 verify the quality and reliability of our model using PyMOL software.

### 143 **Identification of TMPRSS2 binding interfaces, selection and characterization of** 144 **SNPs**

145 Although there is not enough information about the active site and the catalytic site of  
146 TMPRSS<sub>2</sub>, by running a protease conserved domain (CD), TMPRSS<sub>2</sub> was analyzed, and  
147 all its link loops residues were predicted with PyMOL. Following the identification of  
148 the binding interfaces, we selected only the variants located at the level of these  
149 connecting loops from the list of missense and damaging TMPRSS<sub>2</sub> SNPs already  
150 predicted and extracted from databases. dbSNP is a database of genetic variants  
151 implemented at the National Center for Biotechnology Information "NCBI" and  
152 GnomAD database were exploited to characterize the selected SNPs (population and  
153 allelic frequency).

### 154 **Homology modelling of selected TMPRSS2 SNPs affecting binding interfaces**

155 To explore the structural changes in the protein encoded by different alleles of  
156 TMPRSS<sub>2</sub>, molecular models of all the selected protein variants were developed and  
157 superimposed over the structurally resolved template of wild-type TMPRSS<sub>2</sub> using  
158 SWISS-MODEL, which allows a fully automated protein structure homology modelling.  
159 The FASTA sequence of TMPRSS<sub>2</sub> was obtained from the UniProt protein knowledge  
160 database (UniProt Id O15393, corresponding to 492 amino acid transcript). The sequence  
161 of each TMPRSS<sub>2</sub> variant is generated at the base of the wild-type sequence by a simple  
162 substitution of the amino acid coding for the missense mutation.

### 163 **Molecular docking**

164 AutoDock Vina was used to carry out the molecular docking between S<sub>1</sub>/S<sub>2</sub> domain of  
165 SARS-CoV<sub>2</sub> spike protein and TMPRSS<sub>2</sub> wild type or missense variants. In our analysis  
166 we used, as a receptor, the TMPRSS<sub>2</sub> wild type or missense variants, and, as a ligand, the  
167 S<sub>1</sub>/S<sub>2</sub> domain of SARS-CoV<sub>2</sub> spike protein model (Code PDB :6ZB4) downloaded from  
168 RCSB-PDB database. To obtain the optimal docking, the interactions of the wild-type  
169 receptor and variants with the partner were simulated using different parameters

170 therefore receptor and ligand we used a grid size was set to 80 × 80 × 80 points with a  
171 spacing of 1 Å.

## 172 **Structure analysis of TMPRSS2 variants and SARS-CoV2 spike protein complexes**

173 To further understand the effect of polymorphisms on receptor recognition by the S<sub>1</sub>/S<sub>2</sub>  
174 domain of SARS-CoV2 a structural analysis was performed by PyMOL. This is an  
175 approach combined with the molecular docking output files to analyze the interactions  
176 between the ligand and its receptor. We evaluate the complexes obtained by docking to  
177 monitor intermolecular hydrogen bonds, electrostatic, and hydrophobic interactions  
178 between SARS-CoV2 S protein and TMPRSS2 missense variants compared to the wild  
179 type.

## 180 **Molecular Dynamics**

181 MD simulations were performed using NAMD<sub>2</sub> as a molecular dynamic program and  
182 VMD as a visualization program to understand the dynamic changes in the  
183 conformations of the wild type and missense variants-domain S<sub>1</sub>/S<sub>2</sub> spike protein  
184 complexes in conditions close to those *in vivo*. MD simulations were carried out in water  
185 for 120 ns at constant temperature of 300 K, using the Langevin dynamics with a damping  
186 constant of 1 ps<sup>-1</sup>. The conformational changes observed during the simulation time  
187 frame are discussed below. Furthermore, VMD was used to determine the stability and  
188 mechanistic aspects of the wild type and mutant complexes by comparing their  
189 corresponding backbone root-mean-square deviation (RMSD), root-mean-square  
190 fluctuations (RMSF) and radius of gyration (Rg).

## 191 **MM-PBSA binding free energy**

192 MD trajectories were used to compute the binding free energy of TMPRSS2 and missense  
193 variants to spike protein, using the molecular mechanics Poisson-Boltzmann solvent  
194 accessible surface area (MM-PBSA) method. This method is one of the most used  
195 approaches to estimate the free energy of binding of small ligands to biological  
196 macromolecules, it has been increasingly used in the study of biomolecular interactions.  
197 The total binding free energy ( $\Delta G_{binding}$ ) can be calculated using Equation 1:

$$198 \quad \Delta G_{binding} = \Delta E_{MM} + \Delta G_{sol} - T\Delta S \quad (\text{Eq. 1})$$

199 The MM/PBSA was used a fast and accurate method to predict the changes of binding  
200 free energy of the protein-protein complex caused by single point mutation. The effect  
201 of the polar and non-polar part of the solvent on the free energy was determined using  
202 the Poisson-Boltzmann equation and calculating the surface area. For our calculation,  
203 the outer dielectric constant was set to 80.0, the inner dielectric constant was set to 1.0,  
204 and the inverse of the grid spacing of 0.5 Å was used, while for the calculation of surface  
205 area, the surface tension value was set to 0.00542 with a surface offset of 0.92. And  
206 finally, the binding energy was summed and averaged over 10 snapshots.

## 207 **RESULTS AND DISCUSSION**

### 208 **Polymorphism and molecular model of human TMPRSS2**

209 To understand the role of TMPRSS2 variants in the infection by SARS-CoV2 virus, we  
210 searched on the Genome Aggregation Database (gnomAD), Ensembl, the 1000 Genomes  
211 Project and NHLBI databases to identify all SNPs in the *TMPRSS2* gene, causing amino  
212 acid changes at the protein level. Within the scoring ranges of the prediction tools, we  
213 identified a total of 692 missense and damaging SNPs with a relatively high allele  
214 frequency between 0.01 and 0.5.

215 Human TMPRSS2 is an 492 amino acid long protein with a transmembrane domain [TM]  
216 (84-106) and three functional domains: an N-terminal LDL-receptor class A domain  
217 [LDLRA] (133-148), followed by the cystein rich domain of the scavenger receptor [SRCR]  
218 (153-246) and finally at C-terminal peptidase S1 domain spanning from 256 to 492 amino  
219 acid which contains the protease active site residues: H296, D345 and S441. The catalytic  
220 domain (C-terminal peptidase S1 domain spanning from 256 to 492) of the crystal  
221 structure of human TMPRSS2, which is the only domain explored in our study, resolved  
222 using I-TASSER, has been aligned with the one recently deposited in the Protein Data  
223 Bank (code PDB: 7MEQ).

224 Figure 1 shows the alignment result of the two structures which shows a strong similarity  
225 between the two domains with an RMSD value equal to 0.705 Å, this proves that our  
226 model is well reliable.

227



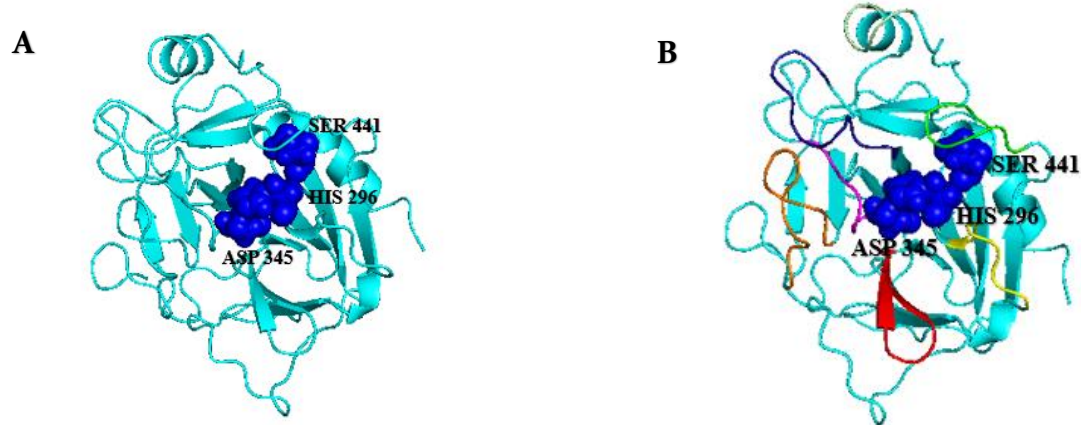


228

229 Figure1: Comparison of the catalytic domain (256-492) of TMPRSS2 modelled by I-  
230 TASSER (shown in Cyan) with the model recently deposited in PDB (code PDB: 7MEQ  
231 shown in Magenta).

### 232 **TMPRSS2 binding interfaces**

233 After obtaining the 3D structure of the TMPRSS2 protein, we mapped the catalytic triad  
234 of TMPRSS2, where residues H296, D345 and S441 were found to be highly conserved  
235 with other protease. Afterward, we predicted seven TMPRSS2 binding loops that may be  
236 involved in the interaction of the S protein with the TMPRSS2 protein, this identification  
237 is based on their position relative the TMPRSS2 protein catalytic triad (Figure 2.A). The  
238 different loops are as follow: Loop1: [Leucine273-Valine283], Loop2: [Valine298-  
239 Asparagine303], Loop3: [Tyrosine337-Asparagine343], Loop4: [Tryptophane384-  
240 Glutamic acid 395], Loop 5: [Serine412-Tyrosine416], Loop6: [Aspartic acid 435-  
241 Aspartic acid 440], Loop 7: [Tryptophane461-Arginine470].



242

243 Figure 2. A) Secondary structure of the catalytic domain of TMPRSS2 protein and the  
244 TMPRSS2 catalytic triad (H296; D345; S441) are shown in blue spheres and B)  
245 Representation of TMPRSS2 protein binding loops.

246 **Polymorphisms of the TMPRSS2 gene related to the protein binding region to**  
247 **the viral particle and geographical distribution of this TMPRSS2 SNPs**

248 The simplest way that missense variation could impact SARS-CoV-2 infection would be  
249 by altering the TMPRSS2-S interface. TMPRSS2 missense variants located at residues  
250 that bind the S protein are most likely to have such effects. In this study, among the 692  
251 natural TMPRSS2 coding variants identified from the different databases, we found that  
252 17 ponctual mutations at positions that have shown to be important for the binding of  
253 TMPRSS2 with the viral spike protein. Furthermore, GnomAD-Exomes database was  
254 used to gain information about frequencies of the examined TMPRSS2 SNPs worldwide.  
255 The population and the frequencies of each TMPRSS2 missense variants are plotted  
256 individually in the Table 1.

257 Table 1: TMPRSS2 SNPs selected with their allele frequencies in each population

258

259

260 **3D structures of the selected variants modelled by SWISS-MODEL**

261 Structurally, all TMPRSS2 variants bear the characteristic domains of TMPRSS2 wild  
262 type. The overall protein architecture of TMPRSS2 allelic variants is largely conserved.  
263 The 3D structure of the 17 TMPRSS2 SNPs presents a significant similarity with the 3D  
264 structure of the wild type and the Ramachandran analysis of the different analogues  
265 proves that all the amino acids of the models are found in the favorable regions.

266 **Molecular docking of SARS-CoV2 S protein and TMPRSS2 wild type or missense**  
 267 **variants**

268 To analyze and quantify the binding affinities and interactions of different models of the  
 269 17 TMPRSS<sub>2</sub> SNPs with the S<sub>1</sub>/S<sub>2</sub> domain of the SARS-CoV<sub>2</sub> S glycoprotein, we

Genomic position	dbSNP	Nucleotide change	Amino acid change	GnomAD	Population
21:41473332	<a href="#">rs747772174</a>	c.1003G>C	<b>Val298Leu</b>	0.00003/31382	African/Asian/European
21:41473332	<a href="#">rs747772174</a>	c.1003G>A	<b>Val298Met</b>	0.00003/31382	African/Asian/European
21:41471871	<a href="#">rs1191785620</a>	c.1010A>G	<b>Tyr337Cys</b>	0.000004/250428	Asian
21:41471865	<a href="#">rs1242962903</a>	c.1016C>T	<b>Ser339Phe</b>	0.000004/250426	European
21:41470668	<a href="#">rs1479410666</a>	c.1151G>T	<b>Trp384Leu</b>	0.00003/32016	*****
21:41470666	<a href="#">rs1213942008</a>	c.1153G>A	<b>Gly385Arg</b>	0.000004/249950	Asian
21:41470660	<a href="#">rs753235785</a>	c.1159A>G	<b>Thr387Ala</b>	0.000008/249842	European/Asian
21:41470653	<a href="#">rs754201785</a>	c.1166A>C	<b>Glu389Ala</b>	0.000008/249730	European
21:41468536	<a href="#">rs1428677799</a>	c.1174A>C	<b>Lys392Gln</b>	0.000004/251348	European
221:41468532	<a href="#">rs1260819364</a>	c.1178C>G	<b>Thr393Ser</b>	0.000004/251364	European
21:41468463	<a href="#">rs1462199231</a>	c.1247A>G	<b>Tyr416Cys</b>	0.000004/251472	American
21:41468407	<a href="#">rs867186402</a>	c.1303G>T	<b>Asp435 Tyr</b>	0.000004/251416	European
21:41468407	<a href="#">rs867186402</a>	c.1303G>A	<b>Asp435Asn</b>	0.000004/251416	European
21:41468398	<a href="#">rs772900547</a>	c.1312C>G	<b>Gln438Glu</b>	0.000004/251368	European
21:41467816	<a href="#">rs936556491</a>	c.1385G>A	<b>Gly462Asp</b>	0.00003/31392	European
21:41467816	<a href="#">rs936556491</a>	*****	<b>Gly462Ser</b>	0.00003/31392	European
21:41467792	<a href="#">rs368268847</a>	c.1409G>T	<b>Arg470Ile</b>	0.00003/31400	African

270 performed 18 docking simulations using AutoDock Vina software of theTMPRSS<sub>2</sub>  
 271 protein and the 17 SNPs with the viral glycoprotein and with the wild type protein and  
 272 obtained the corresponding protein-ligand complexes. The binding energies are  
 273 determined and reported in kcal/mol units in Table 2, which represents the binding

274 energy of the best model identified with the docking software. Our docking simulations  
275 showed that TMPRSS2 and missense variants have high binding affinities with the  
276 domain S<sub>1</sub>/S<sub>2</sub> of spike protein. Overall, the variants have a slightly higher interaction  
277 energies (0.3 to 1.1 kcal/mol) in respect to the wild type protein.

278 **Table 2: Molecular docking results of the TMPRSS2 wild type and the corresponding 17**  
279 **SNPs with the viral S protein**

Protein position	Reference residue	Altered residue	Energy (kcal/mol)
TMPRSS2	wild type	wild type	-13.8
438	Q	E	-14.9
462	G	S	-14.7
462	G	D	-14.9
385	G	R	-14.6
387	T	A	-14.5
389	E	A	-14.9
392	K	Q	-14.9
393	T	S	-14.5
416	Y	C	-14.5
435	D	Y	-14.7
435	D	N	-14.7
470	R	I	-14.6
298	V	L	-14.3
298	V	M	-14.1
337	Y	C	-14.4
339	S	F	-14.9
384	W	L	-14.5

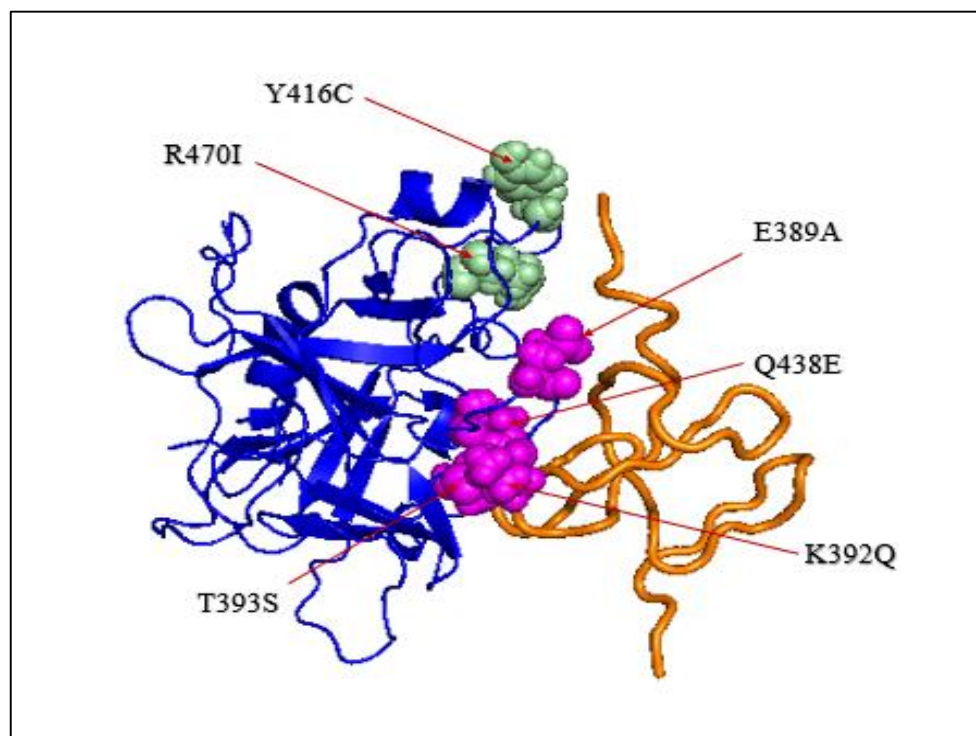
280

### 281 **Missense variants impact on binding of TMPRSS2 receptor to the viral S protein**

282 Firstly, the interaction of wild type TMPRSS2 and the selected missense variants with  
283 the 3D structure of spike monomer protein were simulated using Autodock Vina.  
284 Additionally, both hydrogen, electrostatic bonds and hydrophobic bonds within  
285 different TMPRSS2-spike protein complexes were assessed using PyMOL. We classified  
286 the polymorphisms into two categories. The first one includes mutations that directly  
287 increase the interaction affinity within the complex, these variants increase the number  
288 of electrostatic interactions or decrease the distance of interaction between the receptor  
289 and ligand residues. We term these mutations as “directly increasing”. The second one

290 includes mutations that directly decrease the interaction affinity of the complex by  
291 decreasing the number of electrostatic interactions or increasing the distance of  
292 interaction between the residues of receptor and its ligand, we term these mutations as  
293 “directly decreasing”. All these mutants were found to affect the residues in the  
294 TMPRSS2/S protein binding interface and in direct contact with the virus domain S<sub>1</sub>/S<sub>2</sub>  
295 residues.

296 Therefore, this structure analysis allowed us to identify four missense variants E389A,  
297 K392Q, T393S and Q438E “directly increasing” the interaction affinity and 2 missense  
298 variants R470I and Y416C “directly decreasing” it.



299  
300 **Figure 3.** Secondary structure of the catalytic domain of TMPRSS2 protein (shown in  
301 blue) and the domain S<sub>1</sub>/S<sub>2</sub> of the SARS-CoV2 (shown in orange). The mutated amino  
302 acids that “directly increasing” are colored in magenta and those “directly decreasing”  
303 are presented as green spheres.

### 304 MD study

305 The complexes of the binding site (255-492) of TMPRSS2 and missense variants with the  
306 spike protein were subject of MD simulation studies over a period of 120 ns to  
307 understand their stability and study the structural consequences of these substitutions.

308 To determine the stability and mechanistic aspects of the wild type and mutant  
309 complexes, hydrogen bond interactions, RMSD, RMSF, Rg and their binding profiles  
310 were analyzed and discussed below.

### 311 **Analysis of RMSD**

312 The RMSD is usually used to measure the protein drift from a reference structure, to  
313 study the residue behavior of the protein during the simulations and to describe the  
314 dynamic stability of systems as it measures the global fluctuations of proteins or  
315 complexes. It reflected the mobility of an atom during the MD simulation trajectory. As  
316 a result, a higher residue RMSD value suggests higher mobility; inversely, a lower residue  
317 RMSD value suggests lower mobility. Therefore, the RMSD analysis was carried out for  
318 the MD simulations of each system to determine the change in the overall stability of  
319 the protein after mutation, more specifically to understand the effect of TMPRSS2  
320 missense variants on the stability of complexes. In addition, we compared the RMSD of  
321 the wild type and mutants TMPRSS2/S protein complexes to the free forms of receptor  
322 (Figure S1) and the wild type complex to mutants TMPRSS2/S protein complexes (Figure  
323 S2) during the 120 ns of MD simulations.

### 324 **Analysis of RMSF**

325 Protein RMSF was plotted to characterize local changes along the protein chain and to  
326 determine the movement of certain amino acid residues around their mean position to  
327 assess the flexibility of the dynamic nature of the residues during amino acid  
328 substitution, as a result, peaks indicate areas of the protein that fluctuated the most  
329 during the molecular dynamic simulation. It is well established that the flexibility  
330 determines the binding like it may not only affect the binding interface between two  
331 interacting partners but also an essential contribution to the entropy penalty during  
332 binding (Tuffery et Derreumaux, 2012).

333 RMSF of all the residues of the binding site (255-492) of the protein in each complex  
334 (TMPRSS2(WT), E389A, K392Q, T393S, Y416C, Q438E and R470I) in comparison to the  
335 RMSF of free forms of receptors have been calculated and plotted in (Figure S3) to

336 understand the role of the amino acid substitution in the interaction with the S<sub>1</sub>/S<sub>2</sub>  
337 domain of Spike protein of SARS-CoV-2.

### 338 **Analysis of gyration radius**

339 Radius of gyration measures the compactness and the dimension of protein-protein  
340 complex during MD simulations that shows the stability of protein folding. We  
341 performed Rg analysis to observe the conformational alterations and dynamic stability  
342 of the TMPRSS<sub>2</sub>(WT)-S<sub>1</sub>/S<sub>2</sub> domain of spike protein and their corresponding mutant  
343 complexes. Data are displayed in Figure S4.

### 344 **Dynamics of hydrogen bonds**

345 Analysis of the hydrogen bonds (HB) during ligand binding is another important factor  
346 that influences protein stability, it has a significant role to strengthen protein-protein  
347 interactions. To elucidate how the mutations affect the TMPRSS<sub>2</sub> and viral protein  
348 interaction at molecular level, the dynamics of hydrogen bonds of each system is  
349 displayed in Figure S5, followed by the evolution of the HB number of each complex and  
350 free forms of the receptor during 120 ns of MD simulations (Figure S6), finishing with a  
351 comparison of the dynamics of hydrogen bonds of each mutant system with the WT  
352 complex (Figure S7).

### 353 **Analysis of the binding free energy**

354 Furthermore, to understand and quantify the strength of the interactions between a  
355 ligand and protein, the binding energies over 10 snapshots is reported as the final  
356  $\Delta G_{\text{binding}}$ . The binding free energy calculation of protein–ligand complexes is necessary  
357 for research into virus–host interactions. Based on the MD simulation trajectories, the  
358 binding free energies of TMPRSS<sub>2</sub> (WT) and selected missense variants to S protein were  
359 calculated using the MM-PBSA method ([Ben shalom et al., 2017](#)) that may ignore the  
360 change in structure of the ligand and the receptor upon ligand binding ([Genheden et](#)  
361 [Ryde, 2015](#)), which may be important factors for the affinity. As a result, the negative  
362 energy of the binding complex shows the strength of the protein–ligand interaction.

363 Table 3 shows a comparison between the free energies of the TMPRSS2 proteins for  
364 SARS-CoV2. Analysis of the results showed that the binding free energy of -39.1 kcal/mol  
365 corresponds to the binding energy of the TMPRSS2 WT which is the highest value  
366 compared to other complexes. In the other hand, the lowest binding free energies of  
367 Q438E, Y416C, T393S, R470I, E389A and K392Q to S1/S2 domain of S protein are -42.7,  
368 -54.0, -61.0, -61.2, -75.1 and -82.8 kcal/mol, respectively. All the variants have a higher  
369 binding energy than the native does, this result suggests that the missense variants have  
370 stronger binding affinity that can be explained by the strong affinity of these variants  
371 towards the S protein compared to the native TMPRSS2.

372 Table 3: MM/PBSA binding free energies (kcal/mol) of wild-type and mutant complexes

Models	Complex	Receptor	Ligand	$\Delta G_{binding}$ (kcal/mol)
Native	-7573.2	-5624.8	-1909.2	-39.1
Q438E	-7601.7	-5667.4	-1891.6	-42.7
Y416C	-7553.3	-5610.1	-1889.2	-54.0
T393S	-7525.9	-5558.9	-1906.0	-61.0
R470I	-7306.2	-5343.4	-1901.5	-61.2
E389A	-7546.5	-5563.6	-1907.8	-75.1
K392Q	-7529.1	-5591.1	-1855.2	-82.8

373

## 374 DISCUSSION

375 Based on recent reports, TMPRSS2 is essential for SARS CoV2 to enter cells, it is one of  
376 the main cell surface proteases involved in the process of S protein priming. However,  
377 to the virus can enter to the cells, a first cleavage of the viral spike protein at the S1/S2  
378 site that is very important for the activation of virus, followed by second cleavage at the  
379 S2' site, which allows viral fusion with the cell membrane and internalization.



380 The gene encoding TMPRSS2 has a high level of genetic variability. In this context (Yuan  
381 et al., 2020), (Ravikanth et al., 2020), (Paniri A et al., 2020), (Senapati S et al., 2020)  
382 suggested that TMPRSS2 DNA polymorphisms were likely to be associated with  
383 susceptibility to COVID-19 and would contribute to differences in SARS-CoV2 infection.  
384 In the other hand, recent studies showed that ACE2 genetic variation is very rare in the  
385 population (Stawiski et al.) (MacGowan and Barton), thus making it a candidate to  
386 explain the inter-individual variability to SARS-CoV2 infection. At present, no disease-  
387 association for TMPRSS2 variants is known. Therefore, we focused on TMPRSS2, which  
388 together with ACE2 plays an important role in SARS-CoV2 infection. Our *in-silico*  
389 analysis of human TMPRSS2 variants was carried out to verify the hypothesis that the  
390 COVID-19 susceptibility is also influenced by genetic variability of gene coding for  
391 TMPRSS2 protein involved in the entry of SARS-CoV-2 into target cells and that certain  
392 populations may be more affected by SARS-CoV2, depending on the frequency of  
393 TMPRSS2 variants. Hence, for further understanding of the susceptibility of individuals  
394 of different populations to SARS-CoV2 and their risk of infection, we analyzed the  
395 1000Genomes, Ensembl, NHLBI, genomAD databases dedicated to mutations to extract  
396 the missense variants of the TMPRSS2 protein. In total, 642 missense variants were  
397 obtained. After modelling the TMPRSS2 3D structure using I-TASSER, we have  
398 compared the catalytic domain of our structure to the one recently deposited in PDB  
399 (code PDB: 7MEQ), which shows a strong similarity with an RMSD value equal to 0.705  
400 Å, then we predicted the binding site with the S1/S2 domain of the S protein. In a further  
401 step, we focused only on the missense variants whose spatial position is at the level of  
402 the binding site in order to identify those that are able to modify the interaction affinity  
403 in a direct way with the S protein.

404 In the present study, we performed an *in-silico* analysis of the SNP variants localized at  
405 the binding loops. Those SNPs can be directly involved in the alteration of interaction  
406 affinity based on molecular docking to obtain the complexes of TMPRSS2. We also  
407 selected missense variants with the viral protein to predict the interaction affinity  
408 between the two partners, followed by a structure function analysis to identify the key  
409 bonds of interaction. In a last step, we carried out a MD study for the wild-type complex  
410 and variants that have the potential to alter the interaction affinity between TMPRSS2

411 and the S protein with aiming to validate the previous results and identify missense  
412 variants of TMPRSS2 that can alter the interaction affinity with the viral protein relative  
413 to the native complex. To determine the stability and mechanistic aspects of the wild  
414 type and mutant complexes, HB interactions, RMSD, RMSF, Rg and their binding  
415 profiles were analyzed.

416 On the other hand, Senapati et al and Ravikanth et al suggested that variants in  
417 TMPRSS2 that are considered damaging by prediction tools may alter the structure of  
418 TMPRSS2 which may indirectly affect the interaction affinity with SARS-CoV2 spike  
419 protein through structural change (Ravikanth et al., 2020; Senapati et al., 2020). Add to  
420 that, Hussein et al performed an *in-silico* study and tested the effect of the frequent  
421 V160M mutation, which is localized at the serine protease domain and suggested that  
422 this mutation can indirectly modify the interaction affinity (Hussein et al.,2020).

423 The results reported in this study show a remarkable change in the interaction affinity  
424 of the missense variants with the spike protein compared to the native protein and  
425 suggest that these missense variants may be directly involved in the modification of  
426 interaction affinity between the human TMPRSS2 protein and SARS-CoV2. The binding  
427 free energy of the 6 SNP variants is higher than that of the native one but the two variants  
428 Y146C and R470I, which are considered by the structure function analysis as decreasing  
429 the binding affinity have a less stable RMSD compared to native, which can decrease the  
430 stability of the two complexes. The R470I is present only in the African population with  
431 an allelic frequency equal to 0.00003 and the Y416C is present only in the American  
432 population with an allelic frequency equal to 0.000004. However, the 4 SNP variants  
433 E389A; K392Q; T393S and Q438E which are considered to increase the interaction  
434 affinity are present only in the European population with allelic frequencies equal to  
435 0.000008;0.000004;0.000004;0.000004, respectively.

## 436 **CONCLUSION:**

437 The COVID-19 pandemic highlighted the functional role of the TMPRSS2 protein in the  
438 priming of the SARS-CoV2 spike protein and the internalization of the virus inside the  
439 host cell. TMPRSS2 is an essential component for viral infection, allowing the activation  
440 of the S protein by cleaving it to generate two distinct fragments. It may therefore be a

441 potential target for the development of therapeutic and preventive approaches. Several  
442 studies have shown the inter-individual variability to SARS-CoV2 infection highlighting  
443 the involvement of demographic, environmental and genetic factors. Natural genetic  
444 variations in the TMPRSS2 gene can modulate the affinity of the interaction of the  
445 TMPRSS2 receptor and the SARS-CoV-2/S protein and lead to a difference in the  
446 susceptibility of the virus response. Our data suggests that certain populations might be  
447 more affected by SARS-CoV2, depending on the frequency of the respective variants.  
448 Overall, the mutations identified in TMPRSS2 human protein binding domain to SARS-  
449 CoV2 had led to structural changes with modification of the interaction affinity between  
450 the TMPRSS2 receptor and spike protein. The RMSD, RMSF, Rg and HB number of the  
451 120 ns simulation run confirms the modification of stability caused by TMPRSS2  
452 missense variants in comparison to the wild type one. The energy calculations reiterate  
453 the binding efficiency of missense variants in comparison to the wild type. Finally, our  
454 results can potentially guide future attempts, to design an inhibitor containing  
455 TMPRSS2 missense variants that are capable of increasing interaction affinity with spike  
456 protein to disrupt the interaction between the TMPRSS2 human protein and SARS-  
457 CoV2.

## 458 **ACKNOWLEDGEMENTS**

459 For computer time, this research (ref. **K1495**) used the resources of the Supercomputing  
460 Laboratory at King Abdullah University of Science & Technology (KAUST) in Thuwal, Saudi  
461 Arabia. The IAU DSR project ID is 2021-113-Sci, The KAUST project ID is K1495 and The  
462 Tunisian federated research project ID is PRFCOV19-D.2P2.

463

## 464 **REFERENCES**

465 1-Auer, P. L., Johnsen, J. M., Johnson, A. D., Logsdon, B. A., Lange, L. A., Nalls, M. A., ... &  
466 Rich, S. S. (2012). Imputation of exome sequence variants into population-based samples and  
467 blood-cell-trait-associated loci in African Americans: NHLBI GO Exome Sequencing  
468 Project. *The American Journal of Human Genetics*, 91(5), 794-808.

469 2- Baughn, L. B., Sharma, N., Elhaik, E., Sekulic, A., Bryce, A. H., & Fonseca, R. (2020,  
470 September). Targeting TMPRSS2 in SARS-CoV-2 infection. In *Mayo Clinic Proceedings* (Vol.  
471 95, No. 9, pp. 1989-1999). Elsevier.

- 472 3- Bhanushali, A., Rao, P., Raman, V., Kokate, P., Ambekar, A., Mandva, S., ... & Das, B. R.  
473 (2018). Status of TMPRSS2–ERG fusion in prostate cancer patients from India: correlation  
474 with clinico-pathological details and TMPRSS2 Met160Val polymorphism. *Prostate*  
475 *international*, 6(4), 145-150.
- 476 4- Böttcher, E., Matrosovich, T., Beyerle, M., Klenk, H. D., Garten, W., & Matrosovich, M.  
477 (2006). Proteolytic activation of influenza viruses by serine proteases TMPRSS2 and HAT from  
478 human airway epithelium. *Journal of virology*, 80(19), 9896-9898.
- 479 5- Berman H, Westbrook J, Feng Z, Gilliland G, Bhat T, Weissig H, Shindyalov I, Bourne P  
480 (2000) The protein data bank.
- 481 6- Ben-Shalom, I.Y.; Pfeiffer-Marek, S.; Baringhaus, K.H.; Gohlke, H. Efficient approximation  
482 of ligand rotational and translational entropy changes upon binding for use in MM-PBSA  
483 calculations. *J. Chem. Inf. Model.* **2017**, 57, 170–189. [[Google Scholar](#)] [[CrossRef](#)].
- 484 7- Chen, N., Zhou, M., Dong, X., Qu, J., Gong, F., Han, Y., ... & Zhang, L. (2020).  
485 Epidemiological and clinical characteristics of 99 cases of 2019 novel coronavirus pneumonia  
486 in Wuhan, China: a descriptive study. *The lancet*, 395(10223), 507-513.
- 488 8-Cunningham, F., Achuthan, P., Akanni, W., Allen, J., Amode, M. R., Armean, I. M., ... &  
489 Cummins, C. (2019). Ensembl 2019. *Nucleicacidsresearch*, 47(D1), D745-D751.
- 490 9- David, A., Khanna, T., Beykou, M., Hanna, G., & Sternberg, M. J. (2020). Structure, function  
491 and variants analysis of the androgen-regulated TMPRSS2, a drug target candidate for COVID-  
492 19 infection. *bioRxiv*.
- 493 10- DeLano, W. L. (2002). Pymol: An open-source molecular graphics tool. *CCP4 Newsletter*  
494 *on protein crystallography*, 40(1), 82-92.
- 495 11- Fu, H., Gumbart, J. C., Chen, H., Shao, X., Cai, W., & Chipot, C. (2018). BFEE: A user-  
496 friendly graphical interface facilitating absolute binding free-energy calculations. *Journal of*  
497 *chemical information and modeling*, 58(3), 556-560.
- 498 12- Genheden, S., & Ryde, U. (2015). The MM/PBSA and MM/GBSA methods to estimate  
499 ligand-binding affinities. *Expert opinion on drug discovery*, 10(5), 449-461.
- 500 13- Hakmi, M., Bouricha, E. M., Akachar, J., Lmimouni, B., El Harti, J., Belyamani, L., &  
501 Ibrahimi, A. (2020). In silico exploration of small-molecule  $\alpha$ -helix mimetics as inhibitors of  
502 SARS-COV-2 attachment to ACE2. *Journal of Biomolecular Structure and Dynamics*, 1-12.  
503
- 504 14-Hussain, M., Jabeen, N., Amanullah, A., Baig, A. A., Aziz, B., Shabbir, S., & Raza, F.  
505 (2020). Structural basis of SARS-CoV-2 spike protein priming by TMPRSS2. *BioRxiv*.  
506
- 507 15-Humphrey, W., Dalke, A., & Schulten, K. (1996). VMD: visual molecular  
508 dynamics. *Journal of molecular graphics*, 14(1), 33-38.

- 509  
510 16-Kumari R, Kumar R, Lynn A. G\_mmpbsa – a GROMACS tool for high-throughput MM-  
511 PBSA calculations. *J Chem Inf Model* 2014; 54:1951-6
- 512 17-Karczewski, K., &Francioli, L. (2017). The genomeaggregationdatabase  
513 (gnomAD). *MacArthur Lab*
- 514 18- Luostari, K., Hartikainen, J. M., Tengström, M., Palvimo, J. J., Kataja, V., Mannermaa, A.,  
515 & Kosma, V.-M. (2014). Type II transmembrane serine protease gene variants associate with  
516 breast cancer. *PLoS*  
517 *One*, 9(7), e102519. <https://doi.org/10.1371/journal.pone.0102519> [[Crossref](#)], [[PubMed](#)], [[Web](#)  
518 [of Science](#) ®], [[Google Scholar](#)]
- 519 19- Matsuyama, S., Nao, N., Shirato, K., Kawase, M., Saito, S., Takayama, ... & Takeda, M.  
520 (2020). Enhanced isolation of SARS-CoV-2 by TMPRSS2 expressing cells. *Proceedings of the*  
521 *National Academy of Sciences*, 117(13), 7001-7003.
- 522 20- Ng, P. C., & Henikoff, S. (2003). SIFT: Predicting amino acid changes that affect protein  
523 function. *Nucleic acids research*, 31(13), 3812-3814.
- 524  
525 21- Paniri, A., Hosseini, M. M., & Akhavan-Niaki, H. (2020). First comprehensive  
526 computational analysis of functional consequences of TMPRSS2 SNPs in susceptibility to  
527 SARS-CoV-2 among different populations. *Journal of Biomolecular Structure and Dynamics*,  
528 1-18.
- 529 22-Phillips, J. C., Braun, R., Wang, W., Gumbart, J., Tajkhorshid, E., Villa, E., ... & Schulten,  
530 K. (2005). Scalable molecular dynamics with NAMD. *Journal of computational*  
531 *chemistry*, 26(16), 1781-1802.
- 532 23-Rentzsch, P., Witten, D., Cooper, G. M., Shendure, J., & Kircher, M. (2019). CADD:  
533 predicting the deleteriousness of variants throughout the human genome. *Nucleic acids*  
534 *research*, 47(D1), D886-D894.
- 535 24-Siva, N. (2008). 1000 Genomesproject
- 536 25-Stawiski, E. W., Diwanji, D., Suryamohan, K., Gupta, R., Fellouse, F. A., Sathirapongsasuti,  
537 F., ... & Seshagiri, S. (2020). Human ACE2 receptor polymorphisms predict SARS-CoV-2  
538 susceptibility. *BioRxiv*.
- 539 26-Senapati, S., Kumar, S., Singh, A. K., Banerjee, P., & Bhagavatula, S. (2020). Assessment  
540 of risk conferred by coding and regulatory variations of TMPRSS2 and CD26 in susceptibility  
541 to SARS-CoV-2 infection in human. *Journal of genetics*, 99, 1-5.

- 542 27- Tuffery, P., & Derreumaux, P. (2012). Flexibility and binding affinity in protein-ligand,  
543 protein-protein and multi-component protein interactions: limitations of current computational  
544 approaches. *Journal of the Royal Society, Interface*, 9(66), 20–  
545 33. <https://doi.org/10.1098/rsif.2011.0584> [[Crossref](#)], [[PubMed](#)], [[Web of Science](#)®], [[Google](#)  
546 [Scholar](#)]
- 547 28-Vishnubhotla, R., Vankadari, N., Ketavarapu, V., Amanchy, R., Avanthi, S., Bale, G., ... &  
548 Sasikala, M. (2020). Genetic variants in TMPRSS2 and Structure of SARS-CoV-2 spike  
549 glycoprotein and TMPRSS2 complex. *BioRxiv*.
- 550 29-Waterhouse, A., Bertoni, M., Bienert, S., Studer, G., Tauriello, G., Gumienny, R., Heer, FT,  
551 de Beer, TAP, Rempfer, C., Bordoli, L., Lepore, R., Schwede, T. SWISS-MODEL: homology  
552 modeling of protein structures and complexes. *NucleicAcidsRes.* 46 (W1), W296-W303  
553 (2018).
- 554 30-Zhang, Y. (2008). I-TASSER server for protein 3D structure prediction. *BMC*  
555 *bioinformatics*, 9(1), 1-8.
- 556
- 557